Use of NMR Spectroscopy in the Synthesis and Characterization of Air- and Water-Stable Silicon Nanoparticles from Porous Silicon

R. S. Carter, S. J. Harley, P. P. Power, and M. P. Augustine*

Department of Chemistry, One Shields Avenue, University of California, Davis, California 95616

Received October 18, 2004. Revised Manuscript Received February 23, 2005

Air- and water-stable silicon nanocrystals were prepared by the bromine oxidation of porous silicon nanoparticles followed by reaction with *n*-butyllithium. Transmission electron microscopy suggests that the vigorous oxidation of porous silicon under reflux conditions removes the porous layer from the nanoparticle to expose a crystalline silicon core that can be passivated with organic ligands. A combination of infrared, ultraviolet/visible, and photoluminescence demonstrate the presence of small crystalline silicon particles and saturated hydrocarbon ligands, while solid- and liquid-state nuclear magnetic resonance spectroscopies establish that butyl ligands are localized on the nanocrystal surface. All of these analytical methods suggest that the product of this synthesis is stable in air and water indefinitely.

Introduction

The synthesis of nanoscale materials is both academically and industrially important.[1,2] A molecular level understanding of the chemistry involved in the preparation of these reduced-scale materials is crucial for the rational fabrication of new commercially viable devices with targeted function.[3] Particularly significant examples are the quantum confinement effects observed in semiconductor nanoparticles,[4] where it has been shown that careful control of particle size can shift the maximum visible luminescence intensity to higher energy,[5−12] a property that has been exploited in the development of sensors,[13] computer displays,[14] and bioinorganic constructs.[15] Although much of the nanoparticle field is focused on using semiconductors such as CdSe, CdS, and InP and inorganic oxides such as SiO_2 and TiO_2, somewhat less information is available for the preparation of pure silicon nanocrystals. Presumably this is due to the different chemistry involved in the synthetic preparation and handling of silicon containing compounds in comparison to the mixed semiconductors and oxides. To date, there are several approaches to fabricating nanocrystalline silicon including the mechanical ball milling of crystalline silicon,[16] chemical vapor deposition,[17] the oxidation of Zintl salts such as Mg_2Si and NaSi,[18] and the reduction of halides such as $SiCl_4$.[19]

The goal of the work reported here is two-fold. The first objective is the gram-scale synthesis of air- and water-stable silicon nanocrystals, while the second is the thorough characterization of the nanoparticle core and surface. In terms of quantity, the most promising approach in this endeavor is the mechanical ball milling method, although the route does not lend itself to reasonable size control or surface passivation. This paper considers the formation of alkyl-passivated silicon nanocrystals from hydride-capped nanoporous silicon np-Si/H[20] followed by surface treatments used in the stabilization of nanocrystals obtained in the oxidative[18] and reductive[19] routes mentioned above. Given the surge of interest in the formation of sensitive optical detectors from np-Si/H,[21] the electrochemical etching of p-type boron doped silicon as shown by

$$\mathrm{Si} + 6\mathrm{HF} \xrightarrow{\mathrm{EtOH}} \mathrm{H_2SiF_6} + \mathrm{H_2} + \text{np-Si/H} + 2\mathrm{H^+} + 2\mathrm{e^-} \quad (1)$$

has been used to prepare hydride-capped porous silicon

* Corresponding author. Fax: +1−530-752-8995. E-mail: augustin@chem.ucdavis.edu.

(1) Heinrich, J. L.; Curtis, C. L.; Credo, G. M.; Kavanagh, K. L.; Sailor, M. J. *Science (Washington, D.C.)* **1992**, *255*, 66.
(2) Delgado, G. R.; Lee, H. W. H.; Pakbaz, K. In *Material Research Society Symposium Proceedings*, **1977**, *471*, 263−268.
(3) Niemeyer, C. M. *Angew. Chem., Int. Ed.* **2001**, *40*, 4128−4158.
(4) Wang, Y.; Herron, N. *J. Phys. Chem.* **1991**, *95*, 525−532.
(5) Takagi, H.; Ogawa, H.; Yamazaki, Y.; Ishizaki, A.; Nakagiri, T. *Appl. Phys.* Lett. **1990**, *56*, 2379−2380.
(6) Zhang, D.; Kolbas, R. M.; Mehta, P.; Singh, A. K.; Lichtenwalner, D. J.; Hsieh, K. Y.; Kingon, A. I. In *Material Research Society Symposium*; MRS: 1992; Vol. 256, pp 35−40.
(7) Schuppler, S.; Friedman, S. L.; Marcus, M. A.; Adler, D. L.; Xie, Y. H.; Ross, F. M.; Chabal, Y. J.; Harris, T. D.; Brus, L. E.; Brown, W. L.; Chaban, E. E.; Szajowski, P. F.; Christman, S. B.; Citrin, P. H. *Phys. Rev. B*: Condens. Matter Mater. Phys. **1995**, *52*, 4910−4925.
(8) Guzelian, A. A.; Katari, J. E. B.; Kadavanich, A. V.; Banin, U.; Hamad, K.; Juban, E.; Alivisatos, A. P.; Wolters, R. H.; Arnold, C. C.; Heath, J. R. *J. Phys. Chem.* **1996**, *100*, 7212−7219.
(9) Dhas, N. A.; Raj, C. P.; Gedanken, A. *Chem. Mater.* **1998**, *10*, 3278−3281.
(10) Yang, C.-S.; Kauzlarich, S. M.; Wang, Y. C. *Chem. Mater.* **1999**, *11*, 3666−3670.
(11) Yang, C.-S.; Bley, R. A.; Kauzlarich, S. M.; Lee, H. W. H.; Delgado, G. R. *J. Am. Chem. Soc.* **1999**, *121*, 5191−5195.
(12) Holmes, J. D.; Ziegler, K. J.; Doty, R. C.; Pell, L. E.; Johnston, K. P.; Korgel, B. A. *J. Am. Chem. Soc.* **2001**, *123*, 3743−3748.
(13) Buriak, J. M. *Chem. Commun.* **1999**, 1051−1060.
(14) Belomoin, G.; Therrien, J.; Smith, A.; Rao, S.; Twesten, R.; Chaieb, S.; Nayfeh, M. H.; Wagner, L.; Mitas, L. *Appl. Phys.* Lett. **2002**, *80*, 841−843.
(15) Acker, J.; Bohmhammel, K.; Henneberg, E.; Irmer, G.; Rover, I.; Roewer, G. *Adv. Mater.* **2000**, *12*, 1605−1610.
(16) Lam, C.; Zhang, Y. F.; Tang, Y. H.; Lee, C. S.; Bello, I.; Lee, S. T. *J. Cryst. Growth* **2000**, *220*, 466−470.
(17) Carosella, C. A.; Schiestel, S.; Stroud, R. M.; Grabowski, K. S.; Kendziora, C.; Stoiber, M. *Nucl. Instrum. Methods Phys. Res., Sect. B* **1999**, *148*, 975−979.
(18) Bley, R. A.; Kauzlarich, S. M. In *Nanoparticles in Solids and Solutions*; Fendler, J. H., Dékány, I., Eds.; Kluwer Academic Press: Dordrecht, The Netherlands, 1996; pp 467−475.
(19) Baldwin, R. K.; Pettigrew, K. A.; Ratai, E.; Augustine, M. P.; Kauzlarich, S. M. *Chem. Commun.* **2002**, 1822−1823.

10.1021/cm040377u CCC: $30.25
Published on Web 04/26/2005

nanoparticles np-Si/H by the sonication of an HF-etched silicon substrate. In this way np-Si/H can be obtained as a starting material for the subsequent liquid-phase oxidative removal of the porous silicon layer via an oxidation reaction such as

$$\text{np-Si/H} + \text{Br}_2 \xrightarrow[\text{reflux}]{\text{hexane}} \text{nc-Si/Br} + \text{Si}_x\text{Br}_y\text{H}_z + \text{HBr} \quad (2)$$

that affords bromide-capped silicon nanocrystals nc-Si/Br and other smaller halide containing silicon polymers $Si_xBr_yH_z$. Further reaction of the nc-Si/Br product with butyllithium BuLi according to

$$\text{nc-Si/Br} + \text{BuLi} \xrightarrow{\text{hexane}} \text{nc-Si/Bu} + \text{LiBr} \quad (3)$$

displaces the bromide capping group leaving butyl-passivated silicon nanocrystals nc-Si/Bu.

In the course of optimizing this synthesis it became clear that the characterization of nc-Si/Bu could be problematic as no analytical technique alone can address the issues of crystallinity, size, and surface passivation. For example, it is well-known that the quantum size effect in semiconductor nanocrystals is manifested as a blue shift in the photoluminescence (PL) spectrum.[22] However, it has been shown in the case of silicon and germanium nanocrystals that this shift is as much a function of the surface passivation and the organization of the nanoparticle surface.[23] For this reason, the PL spectrum alone is not adequate proof of the formation of stable surface-passivated silicon nanoparticles.[24] The ultraviolet/visible (UV/vis) absorption or transmission spectra of surface-passivated nanomaterials suffer a similar fate as the observed results could be due to quantum confinement, surface morphology, or the chemical composition of the surface passivation agent.[25] Although infrared or Fourier transform infrared (FTIR) spectroscopy can be used to identify vibrations between the nanoparticle and the surface ligand,[26] no information on the crystallinity or size typically determined by transmission electron microscopy (TEM) is obtained.[27] Furthermore, the vibrations of interest in the FTIR spectra are usually obscured by bands corresponding to other molecular components of the passivated nanoparticle. In many nanoscience applications the limitations of each of these characterization methods lead to confusing inconsistent results, a situation that may lead to inaccurate predictions of material properties and structure. Although nuclear magnetic resonance (NMR) spectroscopy is routine in the structure determination of small molecules and <30 kDa proteins and nucleic acids, to date nanoscience applications are limited. This is in large part due to the lack of available standard spin $I = 1/2$ isotopes such as ^{13}C, ^{1}H, and ^{31}P, etc., in the nanoparticle core combined with the slow >0.1 μs correlation time for molecular tumbling appropriate for >10 nm diameter particles dispersed in solution.[28] Here broad featureless signals can result for nanoparticles with $I = 1/2$ nuclei translating into limited site-dependent chemical shift dispersion, a situation that makes standard NMR structure determination strategies useless. Alternate methods that instead use scalar J couplings between less standard $I = 1/2$ spins such as ^{29}Si and ^{13}C for silicon nanoparticles, relaxation parameters for $I > 1/2$ spins such as ^{113}In in the indium phosphide nanoparticles, or the complete removal of solvent followed by application of solid-state NMR must be pursued. This study uses all of the usual material characterization methods mentioned above and endeavors to highlight the role of both multinuclear liquid- and solid-state NMR spectroscopy to probe $^{29}Si-^{13}C$ scalar J couplings and $^{1}H-^{29}Si$ through-space dipolar couplings to respectively study the relationship between the nanoparticle bulk and surface ligands in butyl-passivated silicon nanocrystals. Therefore, consistent with the structure determination of organic, inorganic, or organometallic chemical compounds, an effective characterization of the nanomaterial necessarily involves a combination of all available analytical tools. Aspects of crystallinity are obtained from a comparison of bright- and dark-field TEM images, particle size estimates can be determined from TEM and PL, and the surface environment can be studied with FTIR and NMR. The next few sections rigorously describe and discuss the preparation of nc-Si/Bu and the application of these analytical techniques to the characterization of nc-Si/Bu.

Experimental Section

Hydride-Capped Porous Silicon Nanoparticles (np-Si/H). np-Si/H was prepared using a modification to established literature procedures.[29] Hydrofluoric acid (HF, 48%); ethyl alcohol (EtOH, 200 proof); *n*-hexane (95%); *n*-pentane (98%); and 8 cm diameter, 526 μm thick, boron-doped 20−30 Ω/cm silicon wafers in the ⟨100⟩ crystal orientation were purchased from Alfa Aesar, Rossville Gold Shield Chemical Co., Acros Organics, Sigma-Aldrich, and Wafer Inc., respectively. To establish a good electrical connection and thus ensure uniform surface etching, aluminum metal was thermally deposited on one side of the silicon wafer so that the opposite polished side of the wafer can be used as the anode in the electrochemical cell shown in Figure 1. Here, one 7.06 cm inner diameter Viton O-ring is pressed on the upper polished face of the silicon wafer, while the lower aluminum-coated side of the wafer is pressed onto a 10 cm diameter disk of aluminum foil that covers another 7.06 cm inner diameter O-ring. In this way a dry electrical contact can be made to the wafer through the aluminum foil. The O-rings also prevent electrolyte leakage from the 2.7 cm deep well created on top of the polished silicon by sandwiching the O-ring/wafer/aluminum foil/O-ring construct between the 15 cm × 15 cm × 2.7 cm PTFE well with a 7 cm diameter hole through the 15 cm × 15 cm face and the 15 cm × 15 cm × 1.2 cm PTFE base plate. Following the addition of approximately 40 mL of a 1:1 48% HF:

(20) Pellegrini, V. T., Alessandro; Mazzoleni, Claudio; Pavesi, Lorenzo *Phys. Rev. B: Condens. Matter Mater. Phys.* **1995**, *52*, 14328−14331.
(21) Liu, R. S., Thomas, A.; Li, Y. Y.; Sailor, M. J.; Fainman, Y. *Sens. Actuators, B* **2002**, *B87*, 58−62.
(22) Alivisatos, A. P. *J. Phys. Chem.* **1996**, *100*, 13226−13239.
(23) Draeger, E. W.; Grossman, J. C.; Williamson, A. J.; Galli, G. *Phys. Rev.* Lett. **2003**, *90* (16), 167402.
(24) Wang, L. R., V.; Blasic, J. *Bioconjugate Chem.* **2004**, *15*, 409−412.
(25) Lee, H. W. H.; Thielen, P. A.; Delgado, G. R.; Kauzlarich, S. M.; Yang, C.-S.; Taylor, B. R. *Crit. Rev. Opt. Sci. Technol.* **2000**, *CR77*, 147−164.
(26) Song, J. H.; Sailor, M. J. *Inorg. Chem.* **1999**, *38*, 1498−1503.
(27) Pettigrew, K. A.; Liu, Q.; Power, P. P.; Kauzlarich, S. M. *Chem. Mater.* **2003**, *15*, 4005−4011.
(28) The rotational correlation time for a spherical particle in solution can be obtained from the Debye expression $4\pi r^3\eta/3kT$, where r is the radius of the particle, η is the viscosity of the solvent, k is the Boltzmann constant, and T is temperature.
(29) Song, J. H.; Sailor, M. J. *J. Am. Chem. Soc.* **1998**, *120*, 2376−2381.

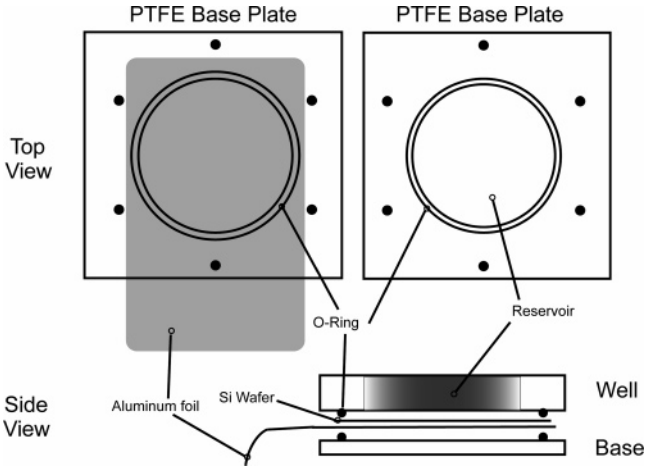

Figure 1. Teflon galvanic reaction cell used in the electrochemical HF mediated etching of crystalline silicon wafers to form np-Si/H nanoparticles. The cell dimensions are 15 cm × 15 cm with a total thickness of 3.5 cm when fully assembled. The aluminum foil is used to create a contact between the aluminum-coated side of the wafer and the externally applied current. The platinum counter electrode is not shown.

EtOH electrolyte solution to the electrochemical cell, a nonreactive platinum cathode is suspended in the electrolyte solution and the aluminum foil in contact with the aluminum-coated surface of the silicon wafer are respectively connected to the negative and positive terminals of a HP 6655A DC power supply. When connected in this way inside a fume hood, a constant 2 A current was maintained through the electrolytic cell to anodically bias the silicon wafer with respect to the platinum counter electrode. Extreme caution should be used when handling the 48% HF solution and when biasing the cell to currents in excess of 2 A. Higher current values may lead to resistive heating and even boiling of the electrolyte solution which emits corrosive/toxic fumes into the fume hood and laboratory. After 25 min of electrochemical etching at an average current density of 52 mA/cm^2, the brown colored etched silicon wafer was removed from the cell, washed with as-received EtOH, and then rewashed with as received *n*-hexane. The np-Si/H was removed from the bulk silicon wafer by submerging the wafer in *n*-hexane and sonicating for 15 min with a Fisher Scientific FS20 sonication bath followed by vigorous scraping with a ceramic spatula. This method isolates the nanoparticulate matter, while leaving the wafer intact for use in another electrochemical etching run. The resulting brown colloidal solution was placed into a Schlenk flask and taken to total dryness. Degassed dry *n*-hexane distilled over sodium was added to the Schlenk flask to redisperse the np-Si/H prior to use in subsequent synthetic steps.

Bromide-Capped Silicon Nanocrystals (nc-Si/Br). Liquid bromine, as received from EM Science, was distilled, degassed, and added to a flask containing hexane-dispersed np-Si/H under argon prepared according to the above procedure. This room-temperature reaction mixture was heated under a positive pressure of argon to reflux and allowed to stir for 2 h until the initial solution lost the red color indicative of unreacted bromine. At this point a gas trap was connected to the reaction flask to collect any excess volatilized bromine and the temperature of the flask was again increased to the reflux condition and allowed to remain constant for 10 h. Finally the temperature of the resulting brown colloid was lowered to room temperature.

Butyl-Capped Silicon Nanocrystals (nc-Si/Bu). An excess of as-received 1.6 M butyllithium in hexanes from Aldrich Chemical Co. was added at 0 °C to the flask containing nc-Si/Br suspended in dry hexane prepared in the previous step. The suspension was stirred for 1 h at 0 °C and then brought to room temperature and allowed to stir for an additional 2 h. The resulting suspension of brown and white particulate matter was placed into a separatory funnel and extracted with ultrapure water to remove any salt impurities and quench excess butyllithium. Following disposal of the aqueous layer, the organic layer was extracted against ultrapure water two more times. The resulting pale yellow hexane solution was taken to dryness, yielding yellow oil that could be converted into a yellow powder by redispersing into dry *n*-pentane and taking to dryness.

Analytical Methods. All infrared spectra were collected with a Mattson Instruments GL-3025 FTIR spectrometer at a resolution of 2 cm^{-1}, and all FTIR samples were prepared by using a stream of argon to dry a drop of hexane-dispersed sample on the surface of a polished KBr sample plate.

Ultraviolet/visible spectra were collected with 2 nm resolution between 190 and 800 nm using a Hewlett-Packard 8452A diode array spectrophotometer. All PL spectra were obtained with a Jobin-Yvon Horiba FluroMax-P PL UV/vis spectrometer. Typically, multiple excitation wavelengths between 300 and 500 nm were used in single-pass mode without signal averaging to determine the maximum PL emission intensity. All UV/vis and PL measurements used quartz 1 cm/side four-sided cells.

All TEM images were obtained with a Phillips CM 12 transmission electron microscope operating at 100 keV. All TEM samples were prepared by drying a drop of hexane-dispersed sample on a holey carbon grid in an oven at 110 °C for 3 h.

All solid-state ^{29}Si and ^{13}C magic angle spinning (MAS) NMR spectra were obtained with use of a Bruker broadband MAS probe capable of handling 4 mm outer diameter O-ring sealed zirconium oxide rotors and interfaced with a home-built NMR instrument controlled by a Tecmag Orion pulse programmer. The respective 58.6 and 74.13 MHz Larmor frequencies correspond to the applied 6.9 T magnetic field generated by an Oxford Instruments superconducting solenoid magnet. In all experiments the sample rotation rate was fixed at 2.5 kHz and the radio frequency (rf) power was adjusted to provide 5 μs $\pi/2$ rf pulses for both the ^{29}Si and ^{13}C channels as well as the 295 MHz Larmor frequency ^{1}H decoupling channel. In this way minimum calibration was required to achieve the ^{1}H−^{29}Si or ^{1}H−^{13}C Hartmann−Hahn side-band matching condition necessary for cross-polarization signal enhancement. Recycle delays of 5 s were used for all cross-polarization experiments, while 240 and 2 s were used when collecting ^{29}Si and ^{13}C Bloch decay spectra, respectively. Measurement of the site-dependent relaxation rates in the laboratory and rotating frame for ^{29}Si and ^{13}C were accomplished with the inversion recovery pulse sequence and by variation of the cross-polarization contact time between ^{1}H and ^{29}Si or ^{13}C, respectively. When necessary, peak intensities were determined by fitting the observed spectrum to a collection of Gaussians. The choice of Gaussian peaks is motivated by the poor signal-to-noise in the observed ^{29}Si NMR spectra that conceals the off-peak wings of the anticipated Lorentzian-shaped NMR lines.

All liquid-phase NMR spectra were collected on a Varian Mercury Plus high-resolution NMR spectrometer housing a 5 mm broadband double resonance probe and operating at Larmor frequencies of 300.06 and 75.46 MHz for ^{1}H and ^{13}C, respectively. In this case the rf power was adjusted on each channel to provide 7 μs ^{1}H and 8.7 μs ^{13}C $\pi/2$ rf pulses. The recycle delays for the observation of ^{1}H Bloch decay and ^{1}H-decoupled ^{13}C NMR spectra were 2 and 10 s, respectively.

Results

Since the primary objective of this work is the multigram synthesis of nc-Si/Bu, it is important to have some quantita-

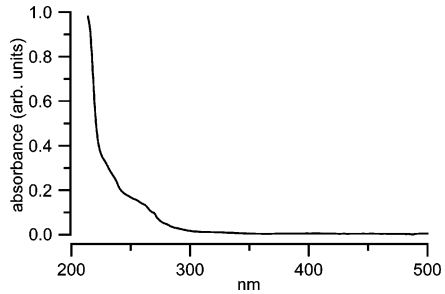

Figure 2. Ultraviolet/visible spectrum of nc-Si/Bu showing the quantum confinement induced shift of the bulk silicon infrared absorption to very short ultraviolet wavelengths.

tive estimate of the yield for all of the reactions mentioned above. The conventional percentage yield for the chemistry reported here obviously cannot be obtained as it is not known how much silicon is converted to small-molecule halides or low molecular weight polymers during bromine oxidation and how many butyl ligands are added to the surface of the nc-Si/Bu particles. What can be estimated is the mass yield of these reactions. One etching run typically yields 0.20 g of np-Si/H. After the np-Si/H is sonicated and removed from the silicon wafer, the wafer can typically be reused one or two more times to afford a total of 0.40−0.60 g of np-Si/H per 8 cm diameter, 5.0 g silicon wafer. Eventually the silicon wafer becomes thin and brittle, which prevents further use. Following bromine oxidation and reaction with butyllithium, the 0.40−0.60 g of np-Si/H are typically converted to 0.13−0.26 g of nc-Si/Bu. Clearly multiple grams of nc-Si/Bu can be obtained by stockpiling the np-Si/H in the first step by etching multiple wafers.

The congested FTIR spectra obtained for np-Si/H and nc−Si/Bu are of limited use for overall chemical structure determination purposes. The only useful information contained in these spectra is the presence of two bands near 2100 cm^{-1} for the np-Si/H sample and the lack of any signals between 2050 and 2150 cm^{-1} for the nc-Si/Bu compound. The UV/vis spectrum for np-Si/H is consistent with the literature,[18] and the spectrum for nc-Si/Bu is shown in Figure 2.

The PL results displayed in Figure 3 for a 300 nm excitation wavelength show the effect of bromine oxidation and butyl surface passivation on np-Si/H. Figure 3a corresponds to the native np-Si/H starting material, while Figure 3b,c were observed 1 min after the room-temperature addition of bromine to np-Si/H followed by butyl capping, and after 10 h at the reflux temperature of hexane followed by butyl capping, respectively. Figure 4 shows the effect of water on the PL spectrum of np-Si/H and nc-Si/Bu. Both Figure 4a,c are appropriate for np-Si/H and nc-Si/Bu in hexane, respectively. Addition of an equal volume of water to these hexane samples followed by 10 min of sonication yields Figure 4b,d for np-Si/H and nc-Si/Bu, respectively. The PL spectra for np-Si/H in Figure 4a,b were generated with 300 nm excitation light, while a 350 nm excitation wavelength was used for the nc-Si/Bu sample in Figures 4c,d.

The bright- and dark-field TEM images for nc-Si/Bu are shown in Figure 5a,b, respectively. A decrease in the length scale from 500 nm in Figure 5 to 200 nm and finally to 50 nm in Figure 6 yields the TEM bright-field images in Figure

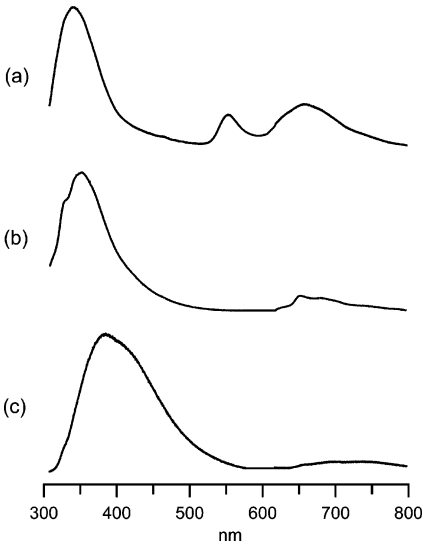

Figure 3. Photoluminescence spectra for np-Si/H before bromine oxidation in a and after 1 min of bromine oxidation in b and 10 h in c. The PL spectra in b and c correspond to the product of the further reaction of nc-Si/Br with butyllithium. All spectra were excited with 300 nm light, and *n*-hexane was used as the solvent.

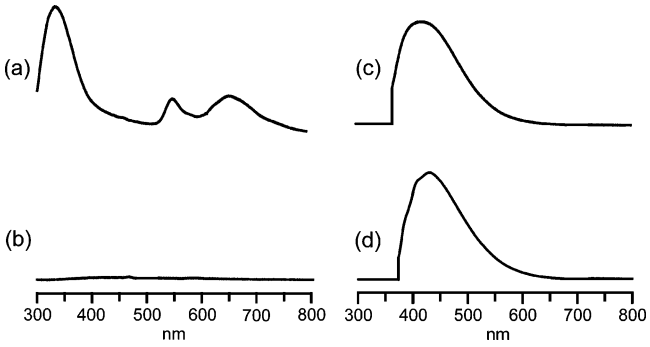

Figure 4. Photoluminescence spectra for np-Si/H in a and nc-Si/Bu in c dispersed in hexane. The addition of an equal volume of water followed by sonication for 10 min yields the PL spectra in b and d for np-Si/H and nc-Si/Bu, respectively. The excitation wavelength in a and b was 300 nm, while in c and d it was increased to 350 nm as evidenced by the windowing function zeroing the data below 375 nm.

6a,c, respectively, and dark-field images in Figure 6b,d, respectively.

Figure 7 shows the three-signal ^{29}Si solid-state NMR spectrum for nc-Si/Bu obtained with ^{1}H cross-polarization. The relaxation properties of each of these signals that are centered at −80, −112, and −120 ppm, were explored by varying the cross-polarization contact time between 0 and 4 ms and by performing a cross-polarization inversion experiment. The slope of the initial magnetization buildup observed when varying the contact time is 10, 100, and 34 ms^{-1} for the signals centered at −80, −112, and −120 ppm, respectively, while the inverted magnetization for these same three signals recovers at 0.04, 0.77, and 1 s^{-1}.

The resolution of the ^{13}C solid-state NMR spectrum with and without cross-polarization was insufficient to resolve any of the four chemical shifts expected for the butyl group on the surface of the nanoparticle. Here, two broad overlapping signals centered in the alkyl ^{13}C chemical shift region and having similar inversion recovery relaxation dynamics were observed. This lack of any useful chemical shift resolution in the solid-state ^{13}C NMR spectrum prompted measurement

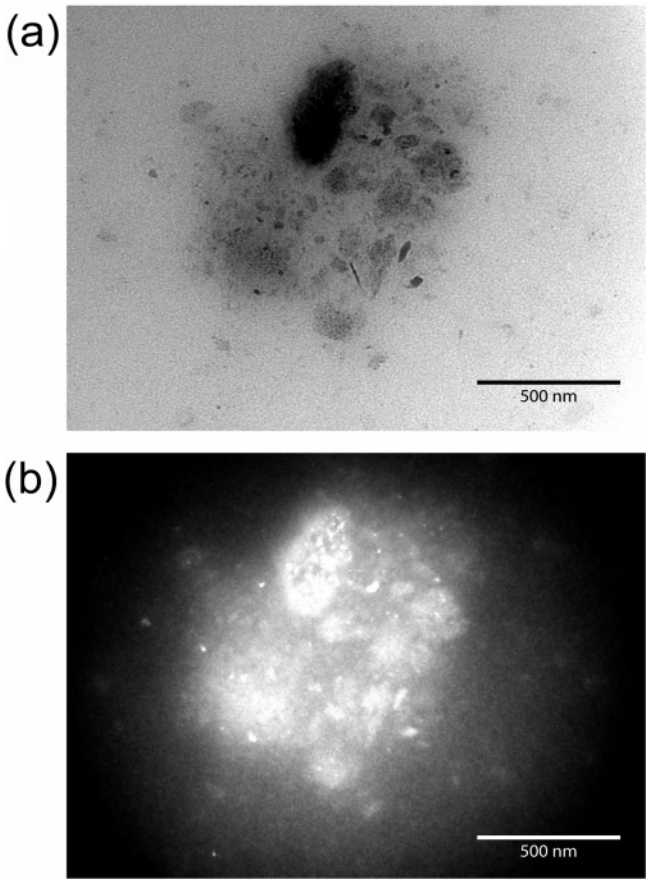

Figure 5. Bright- (a) and dark-field (b) TEM images of nc-Si/Bu using a 500 nm scale. The dark-field image shows the presence of crystalline material.

of the liquid-phase ^{13}C spectrum for nc-Si/Bu shown in Figure 8. The asterisks denote impurities, while the four signals at 8.9, 13.8, 27.6, and 29.5 ppm earmark the four carbons anticipated for the butyl capping group. Careful inspection of the spectrum in Figure 8 reveals that each peak contains two *J* couplings, with the most obvious 450 and 458 Hz splittings of the signal centered at 8.9 ppm.

Discussion

The FTIR, UV/vis, PL, and TEM data shown in Figures 2−6 strongly suggest that air- and water-stable butyl-capped silicon nanocrystals nc-Si/Bu can be synthesized by bromine oxidation of np-Si/H followed by surface passivation with butyllithium. The doublet at 2100 cm^{-1} in the FTIR spectrum for np-Si/H is assigned as a ν_{Si-H} stretch consistent with the literature involving hydride-passivated porous and nanocrystalline silicon.[29] The lack of any signal in the FTIR spectrum for nc-Si/Bu in the region between 2050 and 2150 cm^{-1} suggests that silicon hydrides have been removed from the np-Si/H surface during the synthesis of nc-Si/Bu. Unfortunately the ν_{Si-C} and ν_{C-H} regions of the spectrum for both the np-Si/H and nc-Si/Br compounds are congested, and no other useful information regarding the surface passivation environment in these materials from FTIR spectroscopy can be gleaned. The UV/vis spectrum for nc-Si/Bu shown in Figure 3 displays quantum confinement effects as the long 1100 nm absorption anticipated for silicon particles with a dielectric constant of the bulk[30] is shifted to much lower wavelengths.

The rather congested FTIR spectra for these materials, combined with the featureless UV/vis spectrum that decays in intensity with longer wavelength, do not provide many critical details regarding nanoparticle size and surface passivation morphology. It is for these reasons that the PL measurements shown in Figures 3 and 4 were performed. The PL spectrum for np-Si/H shown in Figure 3a is consistent with the literature, namely, the two primary emission wavelengths are orange and blue with a secondary green emission.[12] In fact, exposure of np-Si/H suspended in hexane to a hand-held, long-pass, ≈365 nm lamp stimulates a brilliant orange luminescence that is visible to the naked eye. The PL spectrum in Figure 3b was obtained after reacting np-Si/H with an excess of bromine at room temperature for 1 min followed by surface passivation with butyllithium. Both the blue band at ca. 340 nm and the orange band at ca. 660 nm persist, while the green emission at ca. 560 nm disappears. This result suggests that after 1 min at room temperature the bromine reacts with readily accessible silicon hydride sites on the np-Si/H surface. Subsequent reaction of these brominated sites with butyllithium yields capped Si−Bu sites and LiBr salt. Figure 3c was obtained after 10 h of refluxing followed by reaction with butyllithium. In this case all three bands in the PL spectrum observed for the starting material np-Si/H in Figure 3b have been replaced by one strong blue emission at ca. 375 nm, luminescence that can be seen with a hand-held, long-pass, ca. 365 nm lamp. In addition to the obvious conclusion that the entire np-Si/H structure has been changed, some more detailed conclusions can be made. A hydride-terminated porous silicon nanoparticle contains an inner crystalline core of silicon encased by an outer noncrystalline layer permeated with cavities having naked or hydride-terminated surface sites with varying degrees of chemical reactivity. It is these sites, in combination with the quantum confinement of bulk crystalline silicon, that lead to the PL spectrum shown in Figure 3a. The decrease in luminescence intensity at ca. 560 nm and ca. 660 nm observed in Figure 3b is consistent with the PL quenching following treatment of np-Si/H with bromine vapor. It was suggested that surface hydrides are displaced by bromine to yield porous bromide-capped silicon nanoparticles np-Si/Br.[31] The PL results shown in Figure 3c suggest that the combination of liquid-phase bromination under severe reflux conditions push the oxidation further by completely stripping the porous layer from the crystalline silicon core, leaving a bromide-capped silicon nanocrystal nc-Si/Br. Subsequent displacement of bromine by butyllithium then affords butyl-capped silicon nanocrystals nc-Si/Bu. It is clear that the prolonged reflux in bromine must be etching the porous layer from the np-Si/H because the direct reaction of np-Si/H with butyllithium simply corresponds to the displacement of the hydride by the butyl group.[29] In fact the PL spectrum for the butyl-capped porous

(30) Franceschetti, A.; Williamson, A.; Zunger, A. *J. Phys. Chem. B* **2000**, *104*, 3398−3401.
(31) Chazalviel, J.-N. O., F. *Mater. Res. Soc. Symp. Proc.* **1999**, *536*, 155−166.

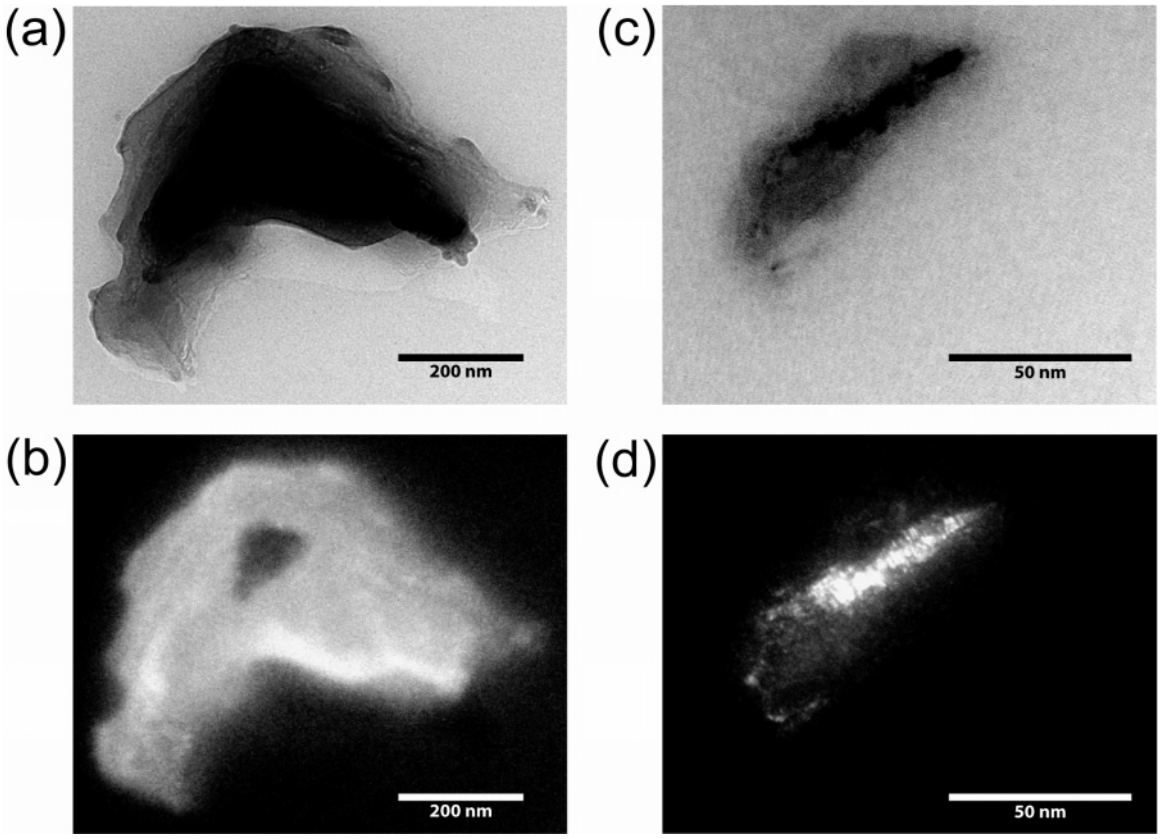

Figure 6. Bright- (a, c) and dark-field (b, d) TEM images of nc-Si/Bu on smaller 200 (a, c) and 50 nm (b, d) scales. These images demonstrate the wide size range of silicon nanocrystals produced by this synthesis.

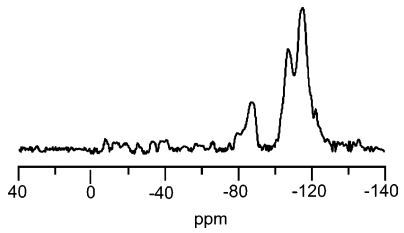

Figure 7. Solid-state ^{29}Si NMR spectrum for nc-Si/Bu. The broad peaks are most likely due to the size heterogeneity inherent in the synthetic approach.

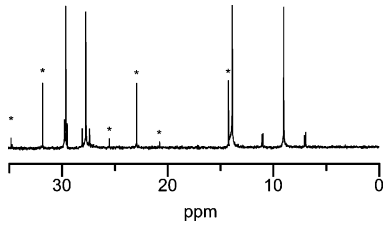

Figure 8. Liquid-state ^{1}H-decoupled ^{13}C NMR spectrum for nc-Si/Bu. The peaks indicated by an asterisk are due to minor impurities.

silicon nanoparticle still contains the signature orange luminescence[29] in contrast to the sole blue emission at ca. 390 nm observed for nc-Si/Bu.

Additional experiments were performed to test for the formation of butyl-capped nanocrystalline silicon. Consider first the surface protection offered to the silicon particle by the butyl capping groups. The PL spectra shown in Figure 4a,c are appropriate for hexane suspensions of np-Si/H and nc-Si/Bu, respectively. Addition of an equal volume of water to these samples, followed by 10 min of sonication, quenches the luminescence in the np-Si/H sample as shown in Figure 4b, while the PL spectrum shown in Figure 4d for the butyl-capped compound nc-Si/Bu is unaffected. The combination of this result, and the formation of a white precipitate in the np-Si/H sample upon water treatment, suggests that water reacts with the silicon hydride on the porous silicon surface and ultimately the crystalline silicon core to produce silicon oxide.[32] The lack of any change in PL and solution characteristics upon the addition of water to the nc-Si/Bu sample in Figure 4c,d indicates that the butyl surface passivation does indeed protect the crystalline silicon core of the nanoparticle. The nc-Si/Bu sample is in fact remarkably stable to water exposure because no change in PL intensity or spectral characteristics was observed after soaking in water in excess of one year.

The PL measurements discussed above suggest complete termination of the silicon nanoparticle and that the particle displays quantum confinement effects, but they do not provide conclusive estimates of the nanoparticle crystallinity or the size distribution. Furthermore, the identity of the surface passivation agent and its relationship to the nanocrystal core remains undefined. In other words, the combination of the reaction conditions with the FTIR, UV/vis, and PL data suggests only that there are small surface-passivated silicon particles suspended in *n*-hexane and that the surface ligands contain carbon. An estimate of the crystallinity and the particle size distribution for nc-Si/Bu can be obtained from the TEM images which are shown in Figures 5 and 6. The bright-field image for nc-Si/Bu, shown in Figure 5a,

(32) Tutov, E. A. P., M. N.; Protasova, I. V.; Kashkarov, V. M. *Tech. Phys. Lett.* **2002**, *28*, 729−731.

suggests that a wide range of particle sizes, with mean diameters between ca. 5 and ca. 400 nm, are produced by this synthesis. The dark-field image shown on the same 500 nm scale in Figure 5b indicates that the material is indeed crystalline. A rough estimate of the nanocrystal size distribution can be obtained by decreasing the field of view to 200 nm, and finally to 50 nm, as shown in the bright- and dark-field images in Figure 6. The presence of crystalline material is again demonstrated in this figure, although the particle size in this particular synthesis can range from less than 5 nm as shown in Figure 6c,d to greater than 200 nm as shown in Figure 6a,b.

Although the presence of small crystalline particles and saturated hydrocarbons is confirmed with the FTIR, UV/vis, PL, and TEM data discussed above, none of these methods provides convincing evidence that the saturated hydrocarbon, here *n*-butyl, is attached to the nanoparticle surface. Two NMR-based methods can be used to establish that the butyl group is in fact tethered to the silicon nanoparticle surface. In the case of the nc-Si/Bu material considered in this study, standard ^{13}C liquid-state NMR spectroscopy provides this information; however, in samples that are impure and/or less well defined, solid-state ^{29}Si and ^{13}C NMR spectroscopies are required. If both liquid- and solid-state NMR spectroscopies are available, then both approaches should be used and complementary results are obtained. The ^{29}Si solid-state NMR spectrum obtained with cross-polarization from ^{1}H is shown in Figure 7. Although it is substantially more time-consuming given the notoriously long relaxation times that plague ^{29}Si NMR spectroscopy, the Bloch decay spectrum (not illustrated here) also displays the same three signals. Each of these signals corresponds to a different chemical environment and given that the chemical shift for ^{29}Si in bulk silicon[33] and the crystalline silicon starting material is -85 ppm, the resonance at -80 ppm is most likely due to the silicon in the interior of the nanoparticle. The two upfield signals at -112 and -120 ppm are then tentatively assigned to chemically distinct surface sites—assignments corroborated by solid-state ^{29}Si NMR relaxation and liquid-state ^{13}C NMR data. Both the laboratory and rotating frame relaxation rates of 0.04 s^{-1} and 10 ms^{-1} for the ^{29}Si peak shown in Figure 7 centered at -80 ppm suggest that the chemical environment is rigid and isolated from the motion of the surface-tethered butyl groups, consistent with the 0.04 s^{-1} laboratory frame relaxation rate for ^{29}Si in the crystalline starting material. The comparatively larger relaxation rates of 0.77 and 1 s^{-1} for the peaks centered at -112 and -120 ppm, respectively, in the ^{29}Si NMR spectrum shown in Figure 7 imply that there is more motional disorder in the vicinity of the surface sites, here due to substitution by the butyl capping group. The proximity of the butyl capping group to the two surface ^{29}Si sites is further evidenced by the increased rotating frame relaxation rates of 100 and 34 ms^{-1} for the ^{29}Si signals centered at -112 and -120 ppm, respectively. This increased rotating frame relaxation rate is to be expected for surface sites as the rate is proportional to the inverse sixth root of the distance between the magnetization source and destination,[34] which, in this case, are the protons on the butyl capping group and the ^{29}Si on the nanoparticle surface. The idea of two chemically distinct exterior ^{29}Si sites on the surface of nc-Si/Bu is further corroborated by the ^{1}H-decoupled ^{13}C NMR spectrum shown in Figure 8. The ^{13}C chemical shifts of 29.5, 27.6, and 13.8 ppm are appropriate for the methylene and methyl groups within the butyl capping group, while the upfield shift of 8.9 ppm for the third methylene carbon is consistent with the upfield chemical shifts observed for ^{13}C bound to ^{29}Si in organosilicon model compounds.[33] In addition, each of these four signals contain two sets of satellites due to scalar *J* coupling to two chemically distinct ^{29}Si sites consistent with the chemical shift and relaxation based assignment of the ^{29}Si solid-state NMR spectrum shown in Figure 7. As expected the size of the $^{29}Si-^{13}C$ scalar *J* couplings decreases as a function of distance from the nanoparticle surface, an observation that leads to the assignment of C1, C2, C3, and C4 for the ^{13}C resonances in Figure 8 centered at 8.9, 27.6, 29.5, and 13.8 ppm, respectively. The intensity of the *J* coupling satellites as well as the 450 and 458 Hz splittings between C1 and the two ^{29}Si surface sites are larger than anticipated in comparison to the satellite intensity and the 50−100 Hz *J* couplings typically observed in organosilicon model compounds.[33] Indeed NMR observables are intimately related to electronic structure.[34] In the case of molecular organosilicon model compounds, the electronic structure reflects the molecular orbitals constructed from atom-centered atomic orbitals, while, for nanoparticles containing in excess of 100 atoms, one must consider the semiconductor band structure. The *J* couplings shown in Figure 8 may in fact reflect penetration of the nanoparticle electronic band into the butyl ligand sphere, thus providing a 4-fold increase in the *J* coupling and aberrant satellite intensities consistent with other unusual effects observed in the NMR spectra of semiconductor materials.[35,3635−36] Clearly, more model materials with varying organic surface passivation must be prepared in order to address this concern—these experiments will be the subject of a future publication.

Finally, consider the relatively large particle size distribution observed in the TEM images shown in Figure 5 which is also manifested in the large line width in the ^{29}Si solid-state NMR spectrum shown in Figure 7. These observations underscore the fact that, although water-stable nc-Si/Bu particles are readily formed with this synthesis, the control over the ultimate size distribution in the current preparation is lacking. There are three ways to control size within the current synthetic methodology. The product of the first synthesis stage np-Si/H is isolated by sonication and wafer scraping. Isolation by just sonication or by filtration or ultracentrifugation of the sonicated/scraped product is one way of tightening the size distribution. Another approach

(33) Mason, J. *Multinuclear NMR*; 1st ed.; Plenum Press: New York, 1987; Vol. 1.

(34) Abragam, A. *The Principles of Nuclear Magnetism*; Oxford University Press: Oxford, U.K., 1961.

(35) Tomaselli, M.; Degraw, D.; Yarger, J. L.; Augustine, M. P.; Pines, A. *Phys. Rev. B*: Condens. Matter Mater. Phys. **1998**, *58*, 8627−8633.

(36) Warren, W. W., Jr.; Norberg, Richard E. *Phys. Rev.* **1967**, *154*, 277−286.

involves the careful control of the temperature and/or the time of the bromine oxidation. Since the porous layer is apparently etched from the np-Si/H in the formation of nc-Si/Br, variations in the oxidation conditions may afford some size control. Finally, the filtration, ultracentrifugation, chromatographic separation, or field flow fractionation[37] approaches typically used to isolate nanoparticles of chosen size may be useful in this endeavor.

Conclusions

Exhaustive analysis of the nc-Si/Bu reaction product suggests that air- and water-stable silicon nanocrystals can be prepared by vigorous bromine oxidation of porous silicon nanoparticles followed by reaction with butyllithium. As suggested in the TEM images, the obvious drawback to this synthetic methodology is the broad size distribution, a problem that can be addressed at various stages throughout the synthesis by chemical and/or mechanical means. The role of multinuclear liquid- and solid-state NMR spectroscopy is critical to the characterization of the passivated reaction product. It is clear that the usual arsenal of analytical techniques is limited to either the nanoparticle core (UV/vis, PL, and TEM) or the surface ligands (UV/vis and FTIR) and no information regarding the relationship of the butyl ligand to the surface is obtained. A similar argument can be made for the role of standard ^{1}H liquid-state NMR spectroscopy in this application where chemical shifts and splittings assign the structure of just the butyl capping group. It is clear from this study that multinuclear ^{29}Si−^{13}C liquid-state and ^{1}H−^{29}Si solid-state NMR spectroscopies serve an equally important role in material characterization as the other analytical methods applied here. Here both scalar J couplings in liquid-dispersed samples as well as through-space dipolar couplings, which are manifested as different ^{1}H−^{29}Si relaxation and magnetization transfer rates, confirm that the butyl ligand is localized on the silicon nanoparticle surface. Although these two NMR-based structural assays are specific for organically passivated silicon surfaces, these or similar approaches will be globally applicable to other common nanoparticle systems, including isotopes such as ^{111}Cd, ^{77}Se, ^{119}Sn, ^{31}P, and ^{197}Au, etc. Additional work will include the development of NMR methods capable of locating the ligand on the nanoparticle surface and the types of surface tethering sites in other common semiconductor assemblies containing these isotopes. From a synthetic perspective, other surface ligands that encourage dispersal of nanocrystalline silicon into water and the chemical attachment of nanocrystalline silicon to biologically useful constructs is planned.

Acknowledgment. Assistance in the acquisition of TEM images at the UC Davis Materials Science Central Facilities from Katherine Pettigrew, support from the NSF under Grant No. CRC-331C, and the use of equipment funded by the NSF under Grant No. DMR-0120990 in Susan M. Kauzlarich's laboratory are gratefully acknowledged. M.P.A. is a David and Lucile Packard and Alfred P. Sloan Foundation fellow.

CM040377U

(37) Schimpf, M. E. *Trends Polym. Sci. (Cambridge, U.K.)* **1996**, *4*, 114−121.